Nucleation of protein fibrillation by nanoparticles

Sara Linse*†‡§, Celia Cabaleiro-Lago*†, Wei-Feng Xue¶, Iseult Lynch*, Stina Lindman‡, Eva Thulin‡, Sheena E. Radford¶, and Kenneth A. Dawson*§

*School of Chemistry and Chemical Biology, and †Conway Institute, University College Dublin, Belfield, Dublin 4, Ireland; ‡Department of Biophysical Chemistry, Lund University Chemical Centre, P. O. Box 124, SE-22100 Lund, Sweden; and ¶Astbury Centre for Structural Molecular Biology, Institute of Molecular and Cellular Biology, Garstang Building, University of Leeds, Leeds LS2 9JT, United Kingdom

Edited by H. Eugene Stanley, Boston University, Boston, MA, and approved March 26, 2007 (received for review February 9, 2007)

Nanoparticles present enormous surface areas and are found to enhance the rate of protein fibrillation by decreasing the lag time for nucleation. Protein fibrillation is involved in many human diseases, including Alzheimer's, Creutzfeld-Jacob disease, and dialysis-related amyloidosis. Fibril formation occurs by nucleation-dependent kinetics, wherein formation of a critical nucleus is the key rate-determining step, after which fibrillation proceeds rapidly. We show that nanoparticles (copolymer particles, cerium oxide particles, quantum dots, and carbon nanotubes) enhance the probability of appearance of a critical nucleus for nucleation of protein fibrils from human β_2-microglobulin. The observed shorter lag (nucleation) phase depends on the amount and nature of particle surface. There is an exchange of protein between solution and nanoparticle surface, and β_2-microglobulin forms multiple layers on the particle surface, providing a locally increased protein concentration promoting oligomer formation. This and the shortened lag phase suggest a mechanism involving surface-assisted nucleation that may increase the risk for toxic cluster and amyloid formation. It also opens the door to new routes for the controlled self-assembly of proteins and peptides into novel nanomaterials.

amyloid | nanotoxicology | surface-assisted nucleation

In the coming decades nanomaterials are considered likely to revolutionize many arenas, including information technology and biomedical industries. Nanomedicine and nanodiagnostics are believed to offer hope with some of the most intractable challenges in human health (1). However, relatively little is known about the potential biological risks from nanoparticles, and growing awareness of these issues has led to the emergence of the field of nanotoxicology (2–4). There is little evidence as yet to imply that nanoscale objects introduce the potential for disease, apart from the long-known induction of the aggressive cancer mesothelioma by nanorods of blue asbestos (5). Many nanoparticles are small enough to access all parts of the body, including the brain (6, 7). Entry into cells can occur via receptor-mediated endocytosis (8), and there is an established *in vivo* link between nanoparticles and reactive oxygen production (9, 10). However, the challenges that these new nanomaterials may present to the organism remain unresolved. Here, we highlight the potential for nanoparticles to promote protein assembly into amyloid fibrils *in vitro* by assisting the nucleation process. Our findings may provide new tools toward an understanding of nucleation mechanisms. We also note that nanoparticles potentially open the door to new routes of controlling biological self-assembly for use in nanomedicine, arising from a novel and general surface-mediated nucleation mechanism.

Nanoparticles are almost invariably coated with proteins when they enter a biological fluid (11–14), with consequent structural and functional perturbations of the surface-bound state of the protein (3). Proteins may be bound in a native-like or denatured form depending on protein surface charge, hydrophobicity, and intrinsic stability, but also depending on particle characteristics (15, 16). Nanoparticles possess enormous surface-to-volume ratios (for example, there is 800 m^2 of surface area per liter of a 1 wt% dispersion of 70-nm particles). The potentially high concentration of proteins adsorbed at the particle surface, combined with the low dimensionality of the surface, can enhance the probability of partially unfolded proteins coming into frequent contact, leading to faster clustering, or even radically new protein clusters (17, 18). These properties of nanoparticles can influence protein self-assembly reactions, with the potential that important biological processes may be perturbed, or that diseases involving protein misfolding and assembly may be enhanced. One important phenomenon involving protein self-assembly is the class of human diseases named amyloidoses. Currently, ≈30 different proteins and peptides are known to cause human amyloid disease (for reviews see refs. 19–23). These diseases involve self-assembly of soluble proteins into large insoluble fibrils through nucleation-dependent assembly, often via the formation of oligomeric structures that possess toxic properties (24, 25). It has been shown that surfaces presented by lipid bilayers (26), collagen fibers (27), polysaccharides (28, 29), and other liquid–air, liquid–solid, or liquid–liquid interfaces (30, 31) can have specific and significant effects in promoting amyloid formation. These observations suggest that interactions with different surfaces could promote protein self-assembly into amyloid fibrils and enhance protein conformational changes associated with other protein misfolding diseases.

Dialysis-related amyloidosis, involving the self-assembly of the human protein β_2-microglobulin (β_2m; Fig. 1), is one of the many known amyloid diseases. It occurs in all patients undergoing long-term hemodialysis (32, 33) and is typified by deposition of amyloid plaques in skeletal tissue (34). β_2m fibril growth occurs via multiple pathways (35, 36), and the fibrils formed through each route have distinct morphology. A seed-independent homogeneous nucleation-and-growth mechanism, requiring high concentration of the monomer only, predominates at pH values <3 (37, 38). Under these conditions the protein is partially or more extensively unfolded, depending on the precise conditions of pH, temperature, and ionic strength (39, 40). Nucleation is a stochastic event, and fibrillation by this mechanism is characterized by a lag phase, after which fibril formation proceeds rapidly to completion. Fibril formation of β_2m has also been observed at neutral pH where the protein is predominantly native (29, 41). At this pH, fibrillation of the wild-type protein

Author contributions: S. Linse, C.C.-L., W.-F.X., I.L., S. Lindman, E.T., S.E.R., and K.A.D. designed research; S. Linse, C.C.-L., W.-F.X., I.L., and S. Lindman performed research; S. Linse, I.L., and E.T. contributed new reagents/analytic tools; S. Linse, C.C.-L., W.-F.X., I.L., S. Lindman, and K.A.D. analyzed data; and S. Linse, S.E.R., I.L., and K.A.D. wrote the paper.

The authors declare no conflict of interest.

This article is a PNAS Direct Submission.

Freely available online through the PNAS open access option.

Abbreviations: NIPAM, *N*-isopropylacrylamide; BAM, *N-tert*-butylacrylamide; β_2m, β_2-microglobulin; SPR, surface plasmon resonance.

See Commentary on page 8679.

§To whom correspondence may be addressed. E-mail: sara.linse@bpc.lu.se or kenneth@fiachra.ucd.ie.

This article contains supporting information online at www.pnas.org/cgi/content/full/0701250104/DC1.

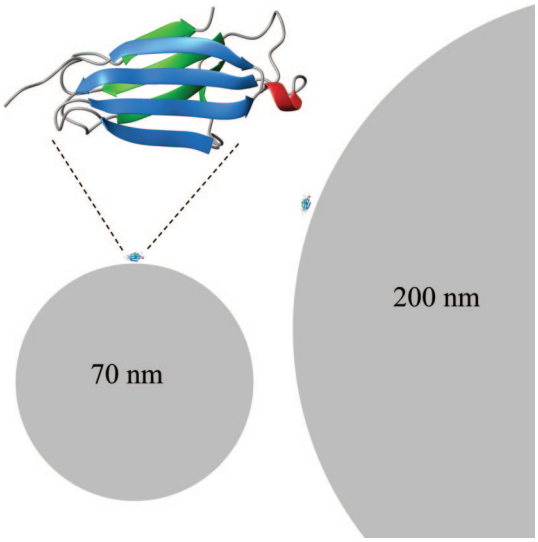

Fig. 1. Size comparison of monomeric β_2m (see *Upper Left* for enlargement) with nanoparticles. One protein molecule is placed on each particle in scale for size comparison with nanoparticles of 70 nm (*Lower Left*) and 200 nm (*Right*). This figure was prepared with Molmol (58).

requires the addition of seeds (29) and is enhanced by SDS (42), glycosaminoglycans (28, 29), and collagen (27). However, the precise molecular mechanism(s) by which these highly charged molecules stimulate assembly is not known.

Here, we show that uncharged polymeric (and other) nanoparticles with different surface properties increase the rate of protein fibril nucleation of β_2m dramatically in the absence of preformed specific seeds. The polymer particles were chosen as models for our studies because they are well controlled in size and purity. They have previously been reported to have low toxicity (43, 44), and similar particles are currently being investigated as drug delivery devices *in vivo* (45). They also allow the size (curvature) and hydrophobicity of the nanoparticle surfaces to be varied systematically, allowing elucidation of the control parameters for nucleation and growth in a novel and powerful manner. To highlight the importance of the issue, and add perspective, we also present results for a selected set of other nanoparticles (quantum dots, carbon nanotubes, and cerium oxide particles) that are intended for early industrial applications of nanotechnology.

Results and Discussion

To examine the role of nanoparticles in protein fibrillation, the self-assembly of β_2m into amyloid-like fibrils was studied at pH 2.5 and 37°C as these conditions lead to the quantitative formation of well characterized amyloid fibrils in the absence of amorphous aggregation (46, 47). The protein concentration was 40, 80, or 125 μM (as determined by absorbance at 277 nm) in 6, 10, or 20 mM sodium phosphate buffer, pH 2.5, at low, 40, or 50 mM NaCl [see supporting information (SI) Table 1]. Under these conditions β_2m is unfolded and lacks residual ordered secondary structure, yet remains compact (R_h increases by ≈20% relative to native β_2m) by virtue of the single disulfide bond that remains intact in the low pH denatured state (40). For all experiments gel filtration was performed immediately before setting up the experiments to isolate the protein monomer and remove any traces of oligomers or aggregates. Buffer stock was added to the monomer solution, the pH was checked on a thoroughly rinsed pH electrode, and the solution was filtered (0.2-μm filter) before incubation at 37°C with or without 0.01 mg/ml copolymer nanoparticles. The resulting solutions correspond to 90 pM 70-nm particles and 4 pM 200-nm particles.

The copolymer particles were made from *N*-isopropylacrylamide (NIPAM) and *N-tert*-butylacrylamide (BAM) at two different ratios of NIPAM/BAM (85:15 or 50:50) and a small amount of cross-linker and were synthesized in SDS micelles to control their size to 70 or 200 nm. Particle sizes were determined by using dynamic light scattering and electron microscopy. The 50:50 NIPAM/BAM nanoparticles are significantly more hydrophobic than the 85:15 NIPAM/BAM particles (44). Particles were dialyzed for several weeks, with the dialysate being checked for conductance until it was the same as pure MilliQ water. The purity of the particles was also checked to ensure the absence of monomer and SDS by NMR (see *SI Text* for further information). Our initial experiments were performed in black 96-well plates and contained four kinds of copolymer nanoparticles (two sizes and two comonomer ratios) in addition to wells without particles. Subsequent experiments were set up in groups of 48–120 samples made from the same solution, some of which were supplemented with the copolymer nanoparticles. For these experiments a 0.5-ml sample was shaken in a 1.5-ml Eppendorf tube at 250 rpm in close to horizontal orientation. To monitor the appearance and growth of fibrils, aliquots from the tubes were taken at different time points, and the fluorescence of thioflavin T was measured. Parallel experiments using intrinsic tryptophan emission or anisotropy as probes showed that the lag times correspond to those measured by using thioflavin T fluorescence.

Our initial experiments at low ionic strength (10 mM sodium phosphate buffer, pH 2.5) in plate format (Fig. 2*A*) showed a dramatic increase in the rate of fibrillation in the presence of nanoparticles. Indeed, fibril formation was completed within ≈1,800 min (in the presence of 85:15 particles) or ≈3,500 min (using 50:50 particles); in the absence of nanoparticles the lag phase is so long that few, if any, fibrils were formed during the 3,500-min time course of this experiment. Negative stain electron microscopy (Fig. 2*B*) shows that the fibrils formed in the presence of particles have a long, straight morphology, which is typical of fibrils formed in the absence of nanoparticles under these conditions (48). Moreover, most of the fibrils are free in solution and not connected to the particles.

To obtain sufficient data for statistical analysis of the effect of the nanoparticles on the growth kinetics and eliminate irreproducibility caused by small differences in solution conditions, a larger collection of 732 experiments with or without copolymer nanoparticles was set up in groups of up to 120 samples in Eppendorf tubes (see *SI Text* for details). One group of 120 samples was set up at the same low-salt conditions as the initial experiments, and all samples with nanoparticles were found to form fibrils more rapidly than those lacking particles (data not shown). The remaining 612 fibrillation experiments were performed at pH 2.5 in the presence of 40 or 50 mM NaCl, under which conditions the rate of fibrillation was increased (35, 47), allowing for the collection of more data in a reasonable time. Under these conditions the presence of 0.01 mg/ml nanoparticles was also observed to enhance the rate of fibrillation, principally by decreasing the length of the lag phase (Fig. 3 *A–D*). By contrast, the rate of fibril elongation appears to be largely unaffected by the presence of the nanoparticles. The relative effect of 70- and 200-nm particles, which differ in total amount of exposed surface area and its curvature, was found to vary with solution conditions such as protein and salt concentration. A complex dependence on protein concentration, exposed surface area, pH, salt concentration, etc. is expected (49).

The detailed molecular mechanism of nucleation on the nanoparticle surface remains elusive, but could involve the particles increasing the probability of homogeneous nucleation events by providing a locally higher concentration of monomers. Alternatively, the interaction with particle surfaces could ac-

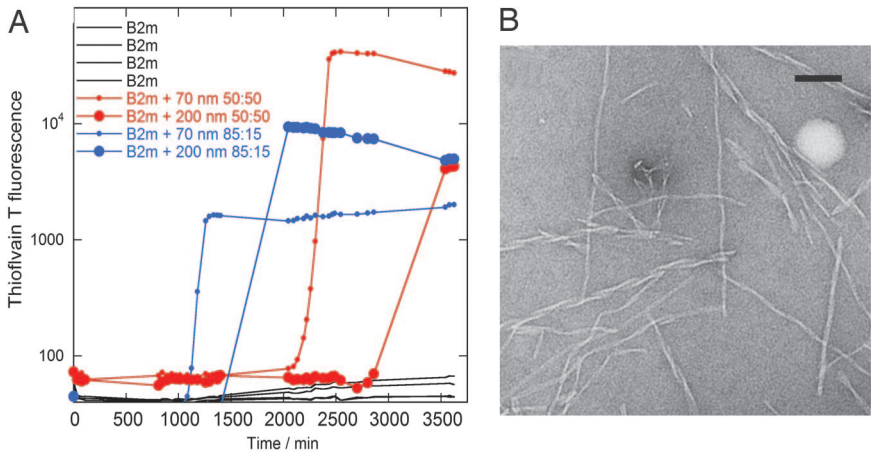

Fig. 2. β_2m fibrillation in the presence of nanoparticles. (*A*) Kinetics of β_2m fibrillation. Thioflavin T fluorescence as a function of time for 80 μM (1 mg/ml) β_2m at 37°C in 10 mM sodium phosphate buffer, pH 2.5, with 0.02% NaN_3, without (black) or with 0.01 mg/ml nanoparticles with 85:15 (blue) or 50:50 (red) NIPAM/BAM ratio is shown. Smaller symbols are used for 70-nm particles. (*B*) Negative stain electron microscopy image of fibers grown in the presence of 70-nm 85:15 NIPAM/BAM copolymer nanoparticles. (Scale bar: 100 nm.)

tively promote an appropriate conformational change. Nonetheless, the dependence of the length of the lag phase on the amount of surface and its characteristics (relative hydrophobicity; Figs. 2 and 3) suggests that the nucleation mechanism involves the association of the protein with the particle surface. To assess the effect of the surface on nucleation in more detail, the interaction of β_2m with the different nanoparticle surfaces was studied by using surface plasmon resonance (SPR). To achieve this, the four kinds of copolymer nanoparticles were immobilized onto gold surfaces by using particles modified to contain a free thiol group (see *SI Text*) (50), and the binding and dissociation of β_2m from the surfaces was monitored (Fig. 4). The total amplitude of the β_2m binding, obtained by curve fitting to the association and dissociation data (see *SI Text*), corresponds to 1×10^5 protein molecules per 200-nm 85:15 particle. A 200-nm particle has a surface area of 1.3×10^{-13} m^2. In its native conformation, β_2m has a cross-sectional area of $0.6–1.3 \times 10^{-17}$ m^2 depending on orientation (it is an oblate spheroid; Fig. 1) meaning that up to 2×10^4 protein molecules would fit in a single layer on a 200-nm particle. At pH 2.5 β_2m is denatured (46) but the hydrodynamic radius of the protein is increased by only 20% (40). Although the results from the SPR are only semiquantitative, they indicate, nonetheless, that several layers of β_2m (but a discrete number) are associated with the particles.

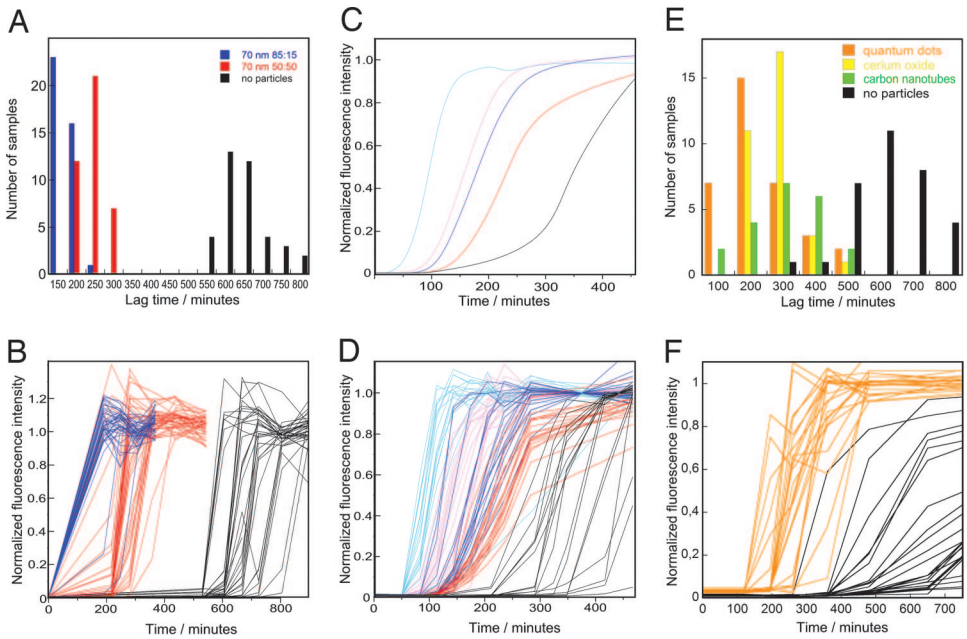

Fig. 3. Kinetics of β_2m fibrillation. (*A* and *E*) Histograms of observed lag times. (*B*, *D*, and *F*) Thioflavin T fluorescence as a function of time showing kinetic traces for all samples in each group. (*C*) The average of all samples of each kind shown in *D*. (*A* and *B*) Forty micromolar β_2m at 37°C in 20 mM sodium phosphate buffer, pH 2.5, with 50 mM NaCl and 0.02% NaN_3. (*C* and *D*) Forty micromolar β_2m at 37°C in 20 mM sodium phosphate buffer, pH 2.5, with 40 mM NaCl and 0.02% NaN_3. (*E* and *F*) Forty micromolar β2m at 37°C in 20 mM sodium phosphate buffer, pH 2.5, with 50 mM NaCl and 0.02% NaN_3. Color coding of kinetic traces and histograms: blue (0.01 mg/ml 70-nm 85:15 NIPAM/BAM particles), cyan (0.01 mg/ml 200-nm 85:15 NIPAM/BAM particles), red (0.01 mg/ml 70-nm 50:50 NIPAM/BAM particles), pink (0.01 mg/ml 200-nm 50:50 NIPAM/BAM particles), orange (100 nM 16-nm quantum dots), green (≤0.01 mg/ml 6-nm-diameter multiwalled carbon nanotubes), yellow (≤0.01 mg/ml 16-nm cerium oxide particles), and black (samples without particles).

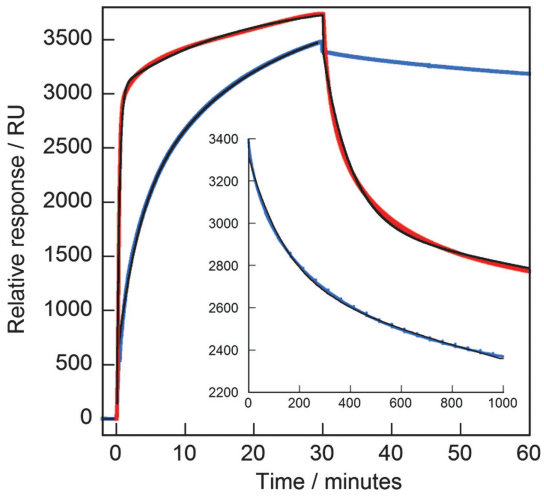

Fig. 4. SPR data for β_2m associating to and dissociating from 200-nm 15:85 NIPAM/ BAM nanoparticles (blue) or 200-nm 50:50 NIPAM/BAM nanoparticles (red) linked to gold via a thiol group. The protein was injected between 0 and 30 min at constant concentration of 40 μM and followed by a constant buffer flow. The black curves were fitted to the association and dissociation data by using Eqs. **1** and **2** in *SI Text*. (*Inset*) An expansion of the dissociation data (blue) with fitted curve (black) for the 200-nm 15:85 NIPAM/BAM nanoparticles.

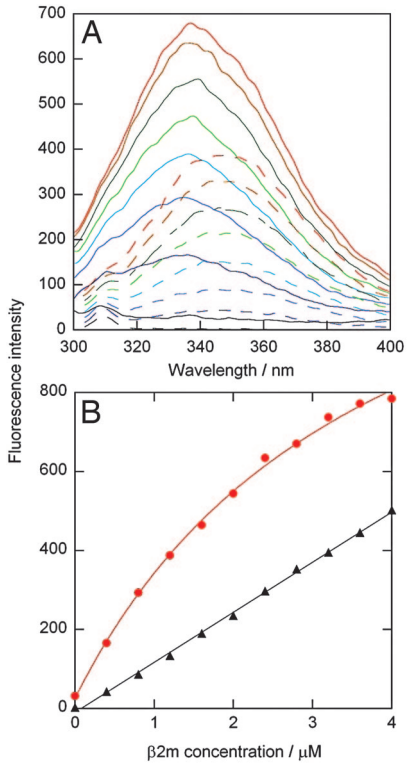

Fig. 5. Change in β_2m conformation in the presence of nanoparticles. (*A*) Trp fluorescence spectra of β_2m titrated into buffer (dashed lines) and into a solution with 70-nm 50:50 NIPAM/BAM nanoparticles (solid lines). (*B*) Fluorescence intensity at 335 nm versus β_2m concentration. β_2m titrated into buffer (black triangles) fitted by a straight line, and β_2m titrated into 70 nm 50:50 nanoparticles (red filled circles) fitted by a 1:1 binding curve is shown.

Two kinetic processes are needed to fit the association and dissociation kinetics obtained from the SPR experiments (see Fig. 4), suggesting that more than one population of β_2m is bound to the surface, in agreement with earlier studies of fibronectin binding to copolymer films (51) and BSA binding to citrate-coated gold nanoparticles (52). The two rate constants for dissociation of β_2m from the 200-nm 85:15 nanoparticles differ by about two orders of magnitude (1×10^{-4} s^{-1} and 2×10^{-6} s^{-1}), whereas the two association rate constants are 20 and 140 M^{-1}·s^{-1}. The rates of dissociation are significantly faster on the more hydrophobic 200-nm particles (off-rate constants 8×10^{-3} s^{-1} and 5×10^{-4} s^{-1}), in agreement with other plasma proteins (50), but the stoichiometry appears to be similar (8×10^4 protein molecules per particle), and the two association rate constants are 15 and 2,000 M^{-1}·s^{-1}, indicating weaker binding to the more hydrophobic surface. We see no variation in the rate constants with particle size (70 or 200 nm).

To analyze the effect of the surfaces on the conformational properties of β_2m, tryptophan fluorescence emission spectra of the protein were acquired in the presence of the different particles. The resulting data revealed an ≈8-nm blue shift in tryptophan fluorescence emission maximum for surface-bound β_2m on the 50:50 NIPAM/BAM particles (Fig. 5), consistent with burial of the tryptophan residues in the more hydrophobic environment of the particle surface. The data for β_2m titrated into the particle solution have the appearance of a binding curve. A simple binding model with a single type of independent sites can be fitted to these data, yielding a stoichiometry of 2,200 ± 1,000 β_2m per 70-nm particle and an apparent affinity of $8 \pm 4 \cdot 10^5$ M^{-1}. The surface of a 70-nm particle would accommodate a maximum of 2,500 protein molecules. The fluorescence data hence suggest that only the innermost layer(s) of particle-bound proteins experiences a blue shift in fluorescence, consistent with burial of Trp toward the hydrophobic groups on the particle surface. This interpretation is supported by the fact that a smaller blue shift is observed with the more hydrophilic 85:15 particles (data not shown). By isothermal titration calorimetry, we observe a positive ΔH, indicating an endothermic process for the binding of the first layer of β_2m that binds to the nanoparticles (Fig. 6), whereas the subsequent layers give no signal (see *SI Text* for experimental details). Thus, for all layers (and predominantly for the innermost layer) association with the nanoparticles is entropy-driven, possibly because of desolvation of the particle and protein surface groups.

The presence of multiple layers of β_2m on the nanoparticles, together with the off-rate constants determined for β_2m from the nanoparticle surfaces, indicates that multiple binding and dissociation cycles occur during the lag phase. These observations provide a rationale by which the particles could enhance the probability of appearance of a critical nucleus (an oligomer or cluster that is in the fibrillation-competent form) for homogeneous (seed-free) nucleation. As a consequence of their hydrophobic nature, therefore, we propose that the nanoparticles enrich the population of protein clusters, and possibly also alter their structural properties (53), thereby enhancing self-assembly. Earlier studies of β_2m in the absence of nanoparticles indicate that fibrillation is preceded by the formation of dimers, trimers, and tetramers (54), although it is not known if any of these oligomers represent the critical nucleus. Further studies of fibrillation using different proteins or peptides, representing several structural classes, combined with systematic alteration of the surface properties of the nanoparticles, therefore, offer a new opportunity to provide molecular insights into the nucleation process itself.

Although this study uses a tailored set of model nanoparticles, it is interesting to ask whether the observed effects also arise with other kinds of nanoparticles, especially those with the most immediately proposed industrial applications. Therefore, we performed one set of 116 experiments in tubes for β_2m alone and in the presence of 16-nm hydrophilic polymer-coated quantum dots (55), 16-nm cerium oxide particles, or multiwalled carbon

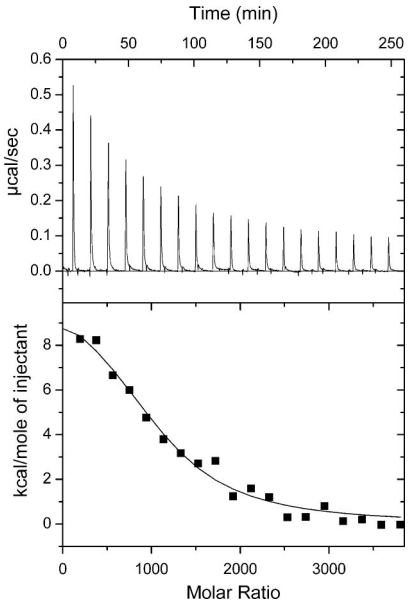

Fig. 6. Isothermal titration calorimetry data at 5°C from titration of β_2m into a solution containing 70-nm 50:50 NIPAM/BAM nanoparticles. The protein concentration was 160 μM, and the particle concentration was 1 mg/ml. Each injection was 15 μl with a total of 19 injections. (*Upper*) Raw data. (*Lower*) integrated data. The black line shows the fitted curve assuming a simple 1:1 binding model with one kind of sites (Eq. **3** in *SI Text*), with the parameter values ΔH = 45 kJ/mol and $K_A = 4 \times 10^5$ M^{-1}, n = 1,040.

nanotubes of 6 nm diameter (56). All of these particles were found to increase the rate of fibrillation by shortening the lag phase (Fig. 3 *E* and *F*), consistent with the view that nucleation is a surface-assisted process.

A wide variety and large amounts of new "surfaces" will flow from the diversity of engineered nanoparticles that are emerging for use in industrial applications, increasing the likelihood of human exposure to nanoparticles. It remains to be seen whether the enormous enhancements in nucleation rate for protein fibrillogenesis demonstrated in this work also occurs *in vivo* or in more complex biological fluids where competitive binding may screen the nucleation surface.

Our findings also suggest other more positive future directions in which nanoparticles could be used to as a "combinatorial" reaction space on which to form new protein assemblies or to enhance and control the rate of protein or peptide self-assembly into amyloid-like materials with novel biotechnological properties as materials with therapeutic roles. Finally, and perhaps most importantly, these particles (by the remarkable amount of control of time scales and cluster enrichment) offer a new and powerful route to define the molecular forces and events that govern protein nucleation mechanisms.

Materials and Methods

Protein. Human β_2m was initially expressed in *Escherichia coli* BL21 pLysS Star from a synthetic gene (with codons optimized for expression in *E. coli*) prepared from overlapping oligonucleotides as described in *SI Text* and SI Fig. 7. The protein was purified from inclusion bodies by using ion exchange steps before and after refolding and one gel filtration step, as described in *SI Text*. Care was taken to avoid deamidation of the protein by limiting the time spent between harvest of the cells and elution from the first exchange column. The gel filtration step was performed to obtain pure monomer just before setting up fibrillation experiments, and any traces of oligomers and aggregates were removed.

Nanoparticles. NIPAM/BAM copolymer particles of 70 and 200 nm diameter and with two different ratios of the comonomers (85:15 and 50:50 NIPAM/BAM) were synthesized in SDS micelles as described by Wu *et al.* (57) with details given in *SI Text*. Hydrophilic polymer-coated quantum dots of 16-nm diameter (55) were provided by W. Parak (Ludwig Maximilians University, Munich, Germany). Cerium oxide particles of 16 nm diameter and multiwalled carbon nanotubes of 6 nm diameter (56) were provided by J. Holmes and M. Morris (University of Cork, Cork, Ireland) and J. Hanrahan of Glantreo Ltd. (Cork, Ireland).

Thiol-Linked Nanoparticles for SPR Studies. NIPAM/BAM/acrylic acid copolymer nanoparticles with maximum one carboxyl group per particle surface were synthesized and modified to provide maximum one thiol group per particle as described in ref. 50 and *SI Text*.

Fibrillation Experiments in Plates. β_2m at 80 μM (1 mg/ml) was incubated at 37°C in 10 mM sodium phosphate buffer, pH 2.5, with 0.02% NaN_3, and 10 μM thioflavin T without or with 0.01 mg/ml nanoparticles in a multiwell plate. The plates were agitated continuously in an incubator at 200 rpm. The thioflavin T fluorescence was measured at 480 nm with excitation at 440 nm.

Fibrillation Experiments in Tubes. In the vast majority of fibrillation experiments, β_2m fibrillation was studied at 37°C in the absence and presence of nanoparticles under a set of solution conditions in Eppendorf tubes. The protein concentration was 40 or 125 μM (as determined by absorbance at 277 nm), in 6, 10, or 20 mM sodium phosphate buffer, pH 2.5, with 0.02% NaN_3, with 0, 40, or 50 mM NaCl. The protein solution was subjected to gel filtration just before setting up the experiments to isolate the protein monomer and remove any traces of oligomers or aggregates. Buffer stock was added to the monomer solution, pH was checked on a thoroughly rinsed pH electrode, and the solution was then filtered [0.2-μm filter (Minisart; Sartorius, Goettingen, Germany), which was washed with buffer before the sample] before it was incubated at 37°C with or without 0.01 mg/ml copolymer nanoparticles. The experiments were set up in groups from the same solution, with 48–120 samples in each group out of which one fraction was without nanoparticles and other fractions were supplemented with nanoparticles. In total, 732 samples were followed for experiments with and without copolymer nanoparticles, and 116 samples were followed in the experiments with and without carbon nanotubes, cerium oxide particles, and quantum dots. Each sample of 0.5 ml was shaken in a 1.5-ml Eppendorf tube at 250 rpm with close to horizontal orientation. To monitor the appearance and growth of fibrils, aliquots from the tubes were taken at different time points and added to a black 96-well plate, and the thioflavin T fluorescence (20 μM thioflavin T added) was measured at 475 nm with excitation at 435 nm in a plate reader.

Electron Microscopy. Negative stain electron microscopy images were taken in a CM-10 microscope (Philips, Eindhoven, The Netherlands). Sample grids were prepared as described (46).

Fluorescence Titrations. β_2m at different concentrations ranging from 0 to 4 μM was mixed with 0.9 nM 70-nm 50:50 or 85:15 NIPAM/BAM particles in 10 mM sodium phosphate buffer, pH 2.5, with 50 mM NaCl and 0.02% NaN_3 at 37°C. Tryptophan fluorescence was excited at 280 nm (slit 2.5 nm), and spectra were recorded between 300 and 420 nm (slit 5 nm), with further details in *SI Text*.

SPR Experiments. Thiol-linked nanoparticles were conjugated to gold as described in ref. 50 and *SI Text*. SPR studies of β_2m associating to and dissociating from surface-tethered nanoparticles were performed with a BIAcore 3000 instrument (BIA-

core, Uppsala, Sweden) at 25°C in 10 mM sodium phosphate buffer, pH 2.5, with 50 mM NaCl as described in *SI Text*. In short, β_2m was injected for 30 min to study the association kinetics. After 30 min, buffer was flown over the sensorchip surface for 10–24 h. The data analysis is described in *SI Text*. In the calculation of the amount of bound proteins per particle, both protein and nanoparticles were assumed to yield a signal of 1 response unit for a bound amount of 1 pg/mm^2.

Isothermal Titration Calorimetry. β_2m was titrated from a 160 μM stock into a 9 nM (1 mg/ml) solution of 70-nm 50:50 or 85:15 NIPAM/BAM nanoparticles in 10 mM sodium phosphate buffer, pH 2.5, with 50 mM NaCl at 5°C. Details and data analysis are given in *SI Text*.

We thank J. Holmes, M. Morris, and J. Hanrahan for carbon nanotubes and cerium oxide nanoparticles and W. Parak for quantum dots. This work was carried out within the original NanoInteract grouping (K.A.D., I.L., and S. Linse) before becoming a European Union FP6 program. It received financial support from Science Foundation Ireland [S. Linse (Walton Fellow), K.A.D., and I.L.], the Swedish Research Council (S. Linse), and the Wellcome Trust (W.-F.X. and S.E.R.).

1. European Commission (2005) *European Technology Platform on NanoMedicine, Vision Paper and Basis for a Strategic Research Agenda for NanoMedicine* (Eur Comm, Brussels).
2. Colvin VL (2003) *Nat Biotechnol* 21:1166–1170.
3. Lynch I, Dawson KA, Linse S (2006) *Science STKE*, 10.1126/stke.3272006pe14.
4. Radomski A, Jurasz P, Alonso-Escolano D, Drews M, Morandi M, Malinski T, Radomski MW (2005) *Br J Pharmacol* 146:882–893.
5. Ramos-Nino ME, Scapoli L, Martinelli M, Land S, Mossman BT (2003) *Cancer Res* 63:3539–3545.
6. Koziara JM, Lockman PR, Allen DD, Mumper RJ (2003) *Pharm Res* 20:1772–1778.
7. Oberdorster G, Sharp Z, Atudorei V, Elder A, Gelein R, Kreyling W, Cox C (2004) *Inhal Toxicol* 16:437–445.
8. Adachi N, Maruyama A, Ishihara T, Akaike T (1994) *J Biomater Sci Polym* 6:463–479.
9. Xia T, Kovochich M, Brant J, Hotze M, Sempf J, Oberley T, Sioutas C, Yeh JI, Wiesner MR, Nel AE (2006) *Nano Lett* 6:1794–1807.
10. Carter JM, Corson N, Driscoll KE, Elder A, Finkelstein JN, Harkema JN, Gelein R, Wade-Mercer P, Nguyen K, Oberdorster G (2006) *J Occup Environ Med* 48:1265–1278.
11. Blunk T, Hochstrasser DF, Sanchez JF, Müller BW, Müller RH (1993) *Electrophoresis* 14:1382–1387.
12. Lück M, Paulke BR, Schröder W, Blunk T, Müller RH (1998) *J Biomed Mater Res* 39:478–485.
13. Gessner A, Waicz R, Lieske A, Paulke B, Mader K, Muller RH (2000) *Int J Pharm* 196:245–249.
14. Labarre D, Vauthier C, Chauvierre C, Petri B, Muller R, Chehimi MM (2005) *Biomaterials* 26:5075–5084.
15. Lundqvist M, Sethson I, Jonsson BH (2004) *Langmuir* 20:10639–10647.
16. Lynch I (2007) *Physica A* 373:511–520.
17. Dawson KA (2002) *Curr Opin Colloid Interface Sci* 7:218–227.
18. Stradner A, Sedgwick H, Cardinaux F, Poon WC, Egelhaaf SU, Schurtenberger P (2004) *Nature* 432:492–495.
19. Koo EH, Lansbury PT, Jr, Kelly JW (1999) *Proc Natl Acad Sci USA* 96:9989–9990.
20. Chien P, Weissman JS, DePace AH (2004) *Annu Rev Biochem* 73:617–656.
21. Westermark P, Benson MD, Buxbaum JN, Cohen AS, Frangione B, Ikeda S, Masters CL, Merlini G, Saraiva MJ, Sipe JD (2005) *Amyloid* 12:1–4.
22. Chiti F, Dobson CM (2006) *Annu Rev Biochem* 75:333–366.
23. Huff ME, Balch WE, Kelly JW (2003) *Curr Opin Struct Biol* 13:674–682.
24. Cleary JP, Walsh DM, Hofmeister JJ, Shankar GM, Kuskowski MA, Selkoe DJ, Ashe KH (2005) *Nat Neurosci* 8:79–84.
25. Baglioni S, Casamenti F, Bucciantini M, Luheshi LM, Taddei N, Chiti F, Dobson CM, Stefani M (2006) *J Neurosci* 26:8160–8167.
26. Knight JD, Miranker AD (2004) *J Mol Biol* 341:1175–1187.
27. Relini A, Canale C, De Stefano S, Rolandi R, Giorgetti S, Stoppini M, Rossi A, Fogolari F, Corazza A, Esposito G, *et al.* (2006) *J Biol Chem* 281:16521–16529.
28. Yamaguchi I, Suda H, Tsuzuike N, Seto K, Seki M, Yamaguchi Y, Hasegawa K, Takahashi N, Yamamoto S, Gejyo F, *et al.* (2003) *Kidney Int* 64:1080–1088.
29. Myers SL, Jones S, Jahn TR, Morten IJ, Tennent GA, Hewitt EW, Radford SE (2006) *Biochemistry* 45:2311–2321.
30. Powers ET, Kelly JW (2001) *J Am Chem Soc* 123:775–776.
31. Lu JR, Perumal S, Powers ET, Kelly JW, Webster JR, Penfold J (2003) *J Am Chem Soc* 125:3751–3757.
32. Gejyo F, Yamada T, Odani S, Nakagawa Y, Arakawa M, Kunitomo T, Kataoka H, Suzuki M, Hirasawa Y, Shirahama T, *et al.* (1985) *Biochem Biophys Res Commun* 129:701–706.
33. Gorevic PD, Casey TT, Stone WJ, DiRaimondo CR, Prelli FC, Frangione B (1985) *J Clin Invest* 76:2425–2429.
34. Floege J, Ehlerding G (1996) *Nephron* 72:9–26.
35. Gosal WS, Morten IJ, Hewitt EW, Smith DA, Thomson NH, Radford SE (2005) *J Mol Biol* 351:850–864.
36. Radford SE, Gosal WS, Platt GW (2005) *Biochim Biophys Acta* 1753:51–63.
37. Naiki H (1997) *Amyloid Int J Exp Clin Invest* 4:223–232.
38. Kad NM, Myers SL, Smith DP, Smith DA, Radford SE, Thomson NH (2003) *J Mol Biol* 330:785–797.
39. McParland VJ, Kalverda AP, Homans SW, Radford SE (2002) *Nat Struct Biol* 9:326–331.
40. Platt GW, McParland VJ, Kalverda AP, Homans SW, Radford SE (2005) *J Mol Biol* 346:279–294.
41. Jahn TR, Parker MJ, Homans SW, Radford SE (2006) *Nat Struct Mol Biol* 13:295–297.
42. Yamamoto S, Hasegawa K, Yamaguchi I, Tsutsumi S, Kardos J, Goto Y, Gejyo F, Naiki H (2004) *Biochemistry* 43:11075–11082.
43. Allen LT, Fox EJ, Blute I, Kelly ZD, Rochev Y, Keenan AK, Dawson KA, Gallagher WM (2003) *Proc Natl Acad Sci USA* 100:6331–6336.
44. Lynch I, Miller I, Gallagher WM, Dawson KA (2006) *J Phys Chem B* 110:14581–14589.
45. Sershen SR, Westcott SL, Halas NJ, West JL (2000) *J Biomed Mater Res* 51:293–298.
46. Kad NM, Thomson NH, Smith DP, Smith DA, Radford SE (2001) *J Mol Biol* 313:559–571.
47. Smith DP, Jones S, Serpell LC, Sunde M, Radford SE (2003) *J Mol Biol* 330:943–954.
48. Ohhashi Y, Hasegawa K, Naiki H, Goto Y (2004) *J Biol Chem* 279:10814–10821.
49. Powers ET, Powers DL (2006) *Biophys J* 91:122–132.
50. Cedervall T, Lynch I, Lindman S, Thulin E, Nilsson H, Dawson KA, Linse S (2007) *Proc Natl Acad Sci USA* 104:2050–2055.
51. Renner L, Pompe T, Salchert K, Werner C (2004) *Langmuir* 20:2928–2933.
52. Brewer SH, Glomm WR, Johnson MC, Knag MK, Franzen S (2005) *Langmuir* 21:9303–9307.
53. Klein J (1986) *J Colloid Interface Sci* 111:305–313.
54. Smith AM, Jahn TR, Ashcroft AE, Radford SE (2006) *J Mol Biol* 364:9–19.
55. Liedl T, Keller S, Simmel FC, Radler JO, Parak WJ (2005) *Small* 1:997–1003.
56. Holmes JD, Lyons DM, Ziegler KJ (2003) *Chemistry* 9:2145–2150.
57. Wu X, Pelton RH, Hamielec AE, Woods DR, McPhee W (1994) *Colloid Polym Sci* 272:467–477.
58. Koradi R, Billeter M, Wüthrich K (1996) *J Mol Graphics* 14:51–55.